01 Mar 1999

Preparation of a ZrO_2-Al_2O_3 Nanocomposite by High-Pressure Sintering of Spray-Pyrolyzed Powders

Rajiv S. Mishra
Missouri University of Science and Technology

V. Jayaram

B. Majumdar

C. E. Lesher

et. al. For a complete list of authors, see https://scholarsmine.mst.edu/matsci_eng_facwork/1478

Recommended Citation

R. S. Mishra et al., "Preparation of a ZrO_2-Al_2O_3 Nanocomposite by High-Pressure Sintering of Spray-Pyrolyzed Powders," *Journal of Materials Research*, Materials Research Society, Mar 1999.
The definitive version is available at https://doi.org/10.1557/JMR.1999.0111

Journal of
MATERIALS RESEARCH

Preparation of a ZrO_2–Al_2O_3 nanocomposite by high-pressure sintering of spray-pyrolyzed powders

R. S. Mishra
Department of Chemical Engineering and Materials Science, University of California, One Shields Avenue, Davis, California 95616

V. Jayaram and B. Majumdar
Department of Metallurgy, Indian Institute of Science, Bangalore 560 012, India

C. E. Lesher
Department of Geology, University of California, One Shields Avenue, Davis, California 95616

A. K. Mukherjee
Department of Chemical Engineering and Materials Science, University of California, One Shields Avenue, Davis, California 95616

(Received 1 November 1996; accepted 30 June 1998)

ZrO_2–Al_2O_3 powders were synthesized by spray pyrolysis. These powders were sintered at 1 GPa in the temperature range of 700–1100 °C. The microstructural evolution and densification are reported in this paper. The application of 1 GPa pressure lowers the crystallization temperature from ~850 to <700 °C. Similarly, the transformation temperature under 1 GPa pressure for $\gamma \rightarrow \alpha$–$Al_2O_3$ reduces from ~1100 to 700–800 °C range, and that for $t \rightarrow m$ ZrO_2 reduces from ~1050 to 700–800 °C range. It was possible to obtain highly dense nanocrystalline ZrO_2–Al_2O_3 composite at temperatures as low as 700 °C. The effect of high pressure on nucleation and transformation of phases is discussed.

I. INTRODUCTION

The ZrO_2–Al_2O_3 system has been widely studied because of its technological importance. Recently, a number of studies have been reported on synthesis and microstructural development in ZrO_2–Al_2O_3 composite by the solution precursor method,[1–5] even though the equilibrium solid solubility of ZrO_2 and Al_2O_3 is very limited. Balmer *et al.*[4] have shown that nanocomposite microstructure develops during heat treatment and these microstructures are extremely stable up to 1000 °C. Briefly, the as-pyrolyzed powder crystallizes upon heat treatment to a single phase tetragonal (t) solid solution which initially phase separates to yield t-ZrO_2 and γ–Al_2O_3 grains of ~20–50 nm. Further heating produces interconnected α–Al_2O_3 plates which grow to a diameter of several microns from a single nucleation event. These plates are interspersed with monoclinic (m) ZrO_2 grains of ~0.1 μm. Such a microstructural scale is stable even after extended heat treatment at 1400 °C. Pressure-assisted densification offers a route to obtain nanometric grains in fully sintered compacts as shown by Mishra *et al.*[6] for the case of nanoscale γ-alumina powders at 1000 °C. If such a route could be adapted to retain fine grain size in coarser powders, the production of dense nanoscale materials would be considerably simplified owing to the low cost, large throughput, and versatility of the solution spray pyrolysis technique.[7] Further, Mishra *et al.*[6] reported that application of 1 GPa pressure reduces the $\gamma \rightarrow \alpha$–$Al_2O_3$ transformation from 1150 to ~750 °C. Jayaram *et al.*[8] have suggested that application of high pressure changes the $\gamma \rightarrow \alpha$–$Al_2O_3$ transformation from a nucleation-controlled process to a growth-controlled one. In this paper we report the microstructural evolution and densification during high pressure sintering of ZrO_2–40 mol % Al_2O_3.

II. EXPERIMENTAL PROCEDURE

Zirconium nitrate and aluminum nitrate were dissolved to a concentration of 200 g/l in the proportion required to yield ZrO_2–40 mol % Al_2O_3. This particular composition is the one reported[4] to show the highest crystallization temperature to form a single phase tetragonal solid solution. The solution was sprayed onto a heated Teflon substrate that was maintained at 200–250 °C. The as-sprayed powder was heat-treated to 500 °C to remove most of the volatiles. Sedimentation analysis indicated an agglomerate size of 7 μm. Compaction was carried out in a Boyd–England apparatus.[9] A schematic diagram of the apparatus is shown in Fig. 1. A green pellet was first prepared by uniaxial compression at 200 MPa. This pellet was then placed at the midpoint of 32 mm long and 6.4 mm inner

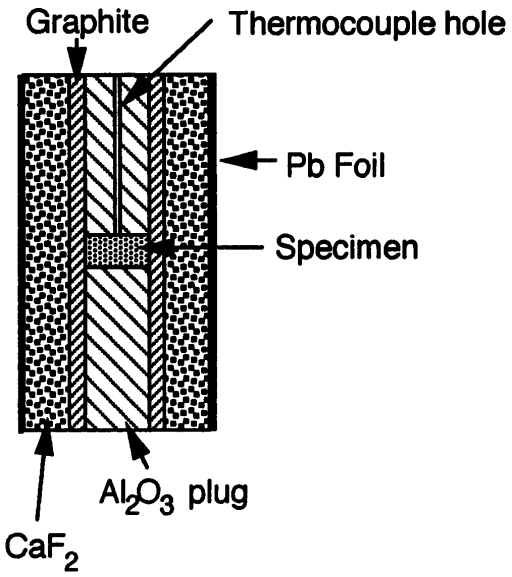

FIG. 1. A schematic illustration of the furnace assembly used for high-pressure sintering.

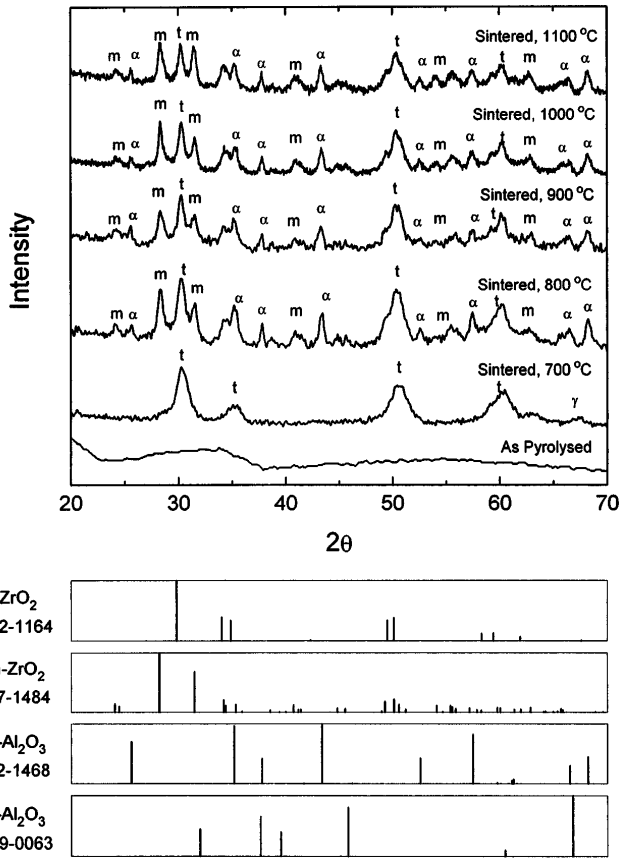

FIG. 2. X-ray diffraction pattern showing evolution of phases during high-pressure sintering at various temperatures. Note that the starting powder does not show any crystalline peak.

diameter cylindrical graphite furnace, surrounded by a sheath of CaF_2 and Pb foil (we would like to point out that the graphite furnace produces a very reducing environment, which could alter the transformation temperatures of metastable phases). The CaF_2 layer acts as a pressure transmitting medium (it crumbles under pressure and transforms uniaxial pressure to quasi-hydrostatic pressure) as well as a thermal barrier. The Pb foil acts as a lubricant for the furnace assembly during the push-out after test. The remaining volume of the furnace is filled by semisintered Al_2O_3 filler rod. A type D (W/Re) thermocouple is placed at the top of the sample and the temperature is regulated using a temperature controller. The sintering was performed by applying 1 GPa pressure on the sample with a heating/cooling rate of 150 K/min and dwell time of 10 min. The samples were analyzed for density (Archimedes principle) and hardness, while characterization was carried out by x-ray diffraction (XRD), nuclear magnetic resonance (NMR), scanning electron microscopy (SEM), and transmission electron microscopy (TEM). ^{27}Al magic angle spinning (MAS) NMR was performed at 104 MHz. The following experimental parameters were used: pulse length = 0.8 μs (nonselective 90° pulse length = 6 μs), pulse delay = 1 s, spinning speed = 15 kHz. Chemical shifts are referenced to external $Al(H_2O)_6^{3+}$ in a 0.1 M $Al(NO_3)_3$ (aq) solution.

III. RESULTS

The results of XRD and MAS-NMR are shown in Figs. 2 and 3, respectively. The pyrolyzed powder is x-ray amorphous while the XRD pattern of the specimen sintered at 700 °C shows the presence of only tetragonal zirconia phase. At 800 °C and above, XRD reveals the presence of *m*-ZrO_2 and $\alpha-Al_2O_3$ while peak splitting due to tetragonality is seen at 900–1100 °C. Between 900 and 1100 °C monoclinic ZrO_2 appears to increase relative to the tetragonal phase, while there is no observable difference in the $\alpha-Al_2O_3$ signals beyond 800 °C except for the reduction in peak broadening which is observed for all phases.

The ^{27}Al MAS-NMR spectrum (Fig. 3) show the presence of 4 (54 ppm), 5 (30 ppm), and 6 (5 ppm) fold coordination in the as-pyrolyzed powder and heat-treated powder. This is different from the expected 4 (66 ppm) and 6 (8 ppm) fold coordination in $\gamma-Al_2O_3$ or 6 (12 ppm) fold coordination in $\alpha-Al_2O_3$.[10] The presence of 4-, 5-, and 6-fold coordination of Al can be attributed to a random distribution of Al ions in the presence of O vacancies in the cubic structure of $\gamma-Al_2O_3$.

It is important to note that 5-fold coordinated sites are not evident in the sintered specimens. At 700 °C, 4-fold (61 ppm) coordinated sites are present in significant amounts. Earlier work[5] has shown that both amorphous as well as crystallized solid solutions of single

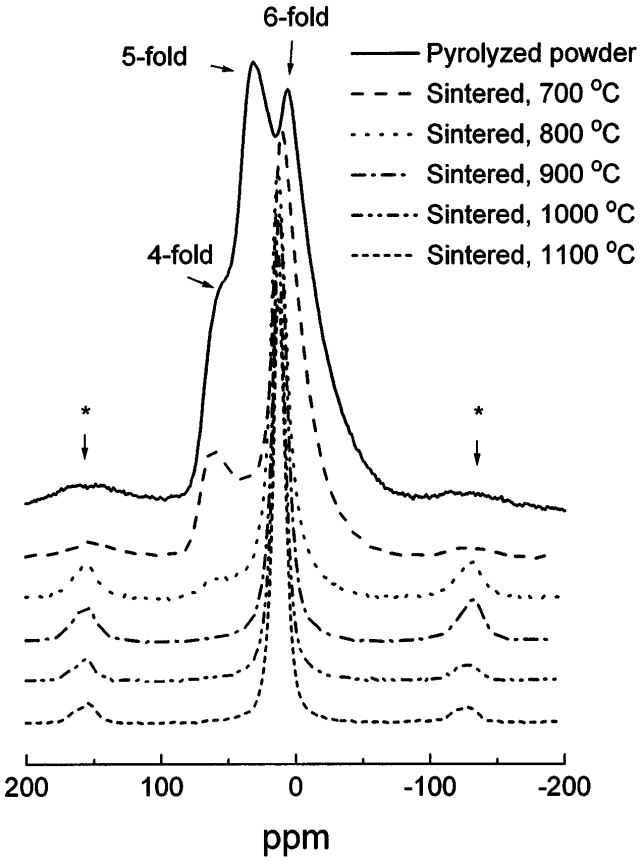

FIG. 3. ^{27}Al MAS NMR spectra for the starting powder and specimens sintered at various temperatures. Note the presence of 5-fold coordination sites in the starting powder. Asterisks denote spinning sidebands.

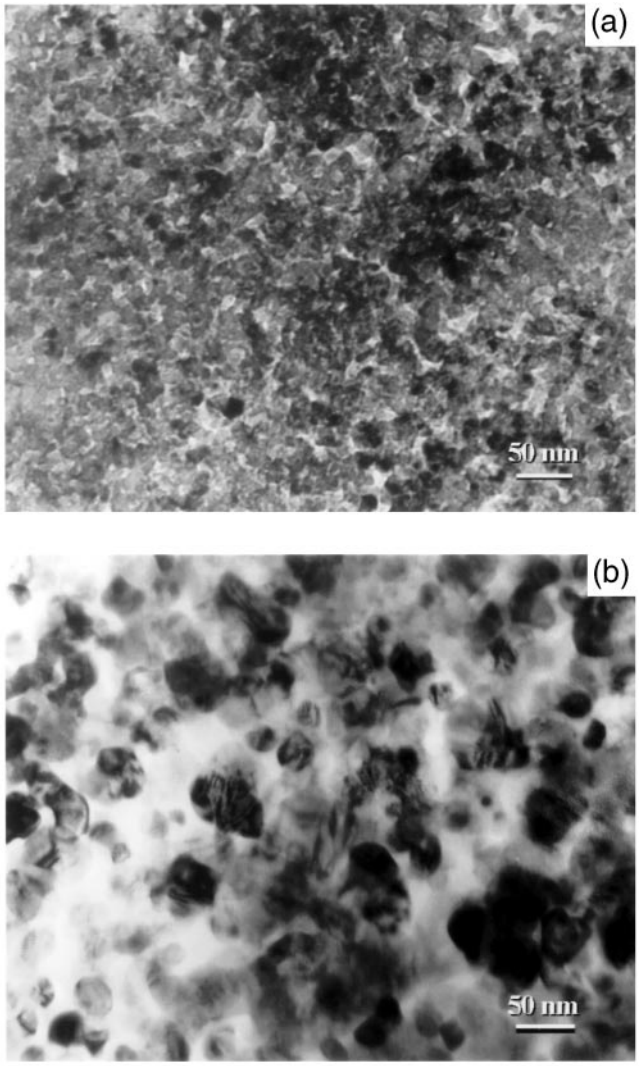

FIG. 4. Transmission electron micrographs of the specimen sintered at (a) 700 °C and (b) 900 °C. No porosity was evident in the specimen sintered at 700 °C (a).

phase $ZrO_2-Al_2O_3$, up to 40 mol% Al_2O_3, display significant 5-fold coordination. In the present experiments, with increase in sintering temperature, 4-fold coordination persists up to 800 °C but disappears after transformation to $\alpha-Al_2O_3$ which has only 6-fold Al coordination. The shift in the 6-fold peak position with sintering, from +5 to +12 ppm is also consistent with transformation of $\gamma \rightarrow \alpha-Al_2O_3$.

Since the major changes in phase content, as revealed by XRD and NMR, occurred in the range 700–800 °C, transmission electron microscopy was carried out on specimens sintered at 700–900 °C. The 700 °C sample displays a more uniform microstructure with much smaller variations in brightness [Fig. 4(a)]. Closer examination indicates a fairly uniform crystallite size of ~20 nm in all regions with no apparent porosity at 700 °C. The low magnification views of the 800 and 900 °C sample revealed a dark, micron-sized particulate with bright intervening regions of ~0.1–0.2 μm. These particulates are likely to be the original agglomerates. Each micron-sized particulate consists of a number of fine grains. The size of individual grains vary from the center to the edge of the particulate. A higher magnification micrograph from the center region of particulate is shown in Fig. 4(b) for a specimen sintered at 900 °C. The grains are in the range of 30–50 nm. The interparticulate regions [Figs. 5(a) and 5(b)] show coarsening with significant residual porosity. For example, Fig. 5(b) shows a three-particle junction with crystallite sizes in the boundary region and in the interior of approximately 0.1 μm and ~20–50 nm, respectively. In particular, these observations of porosity in the interparticulate regions at 800 and 900 °C suggest that the cause is not desintering of a densified region during the gamma-to-alpha transformation, but rather due to incomplete densification of powders. Selected area diffraction patterns at 700 °C (Fig. 6) reveal strong rings corresponding to the fluorite structure with a lattice parameter of 5.12 Å. However, additional weak rings are present for

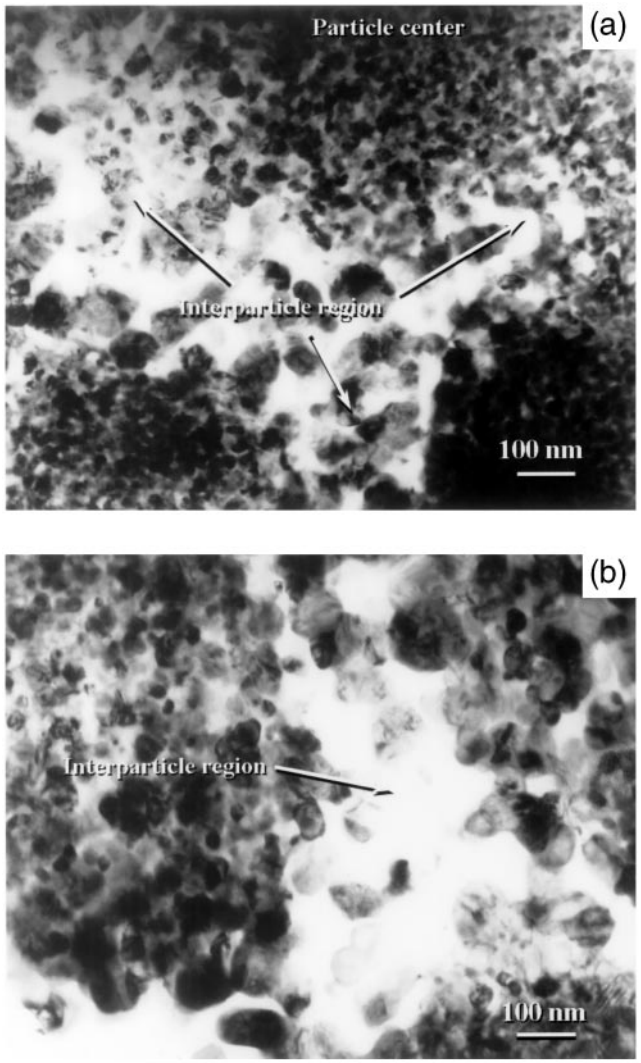

FIG. 5. High magnification transmission electron micrographs of the interparticle region (particle junction) sintered at (a) 800 °C and (b) 900 °C. The particle junctions showed areas with porosity and relatively bigger grain sizes.

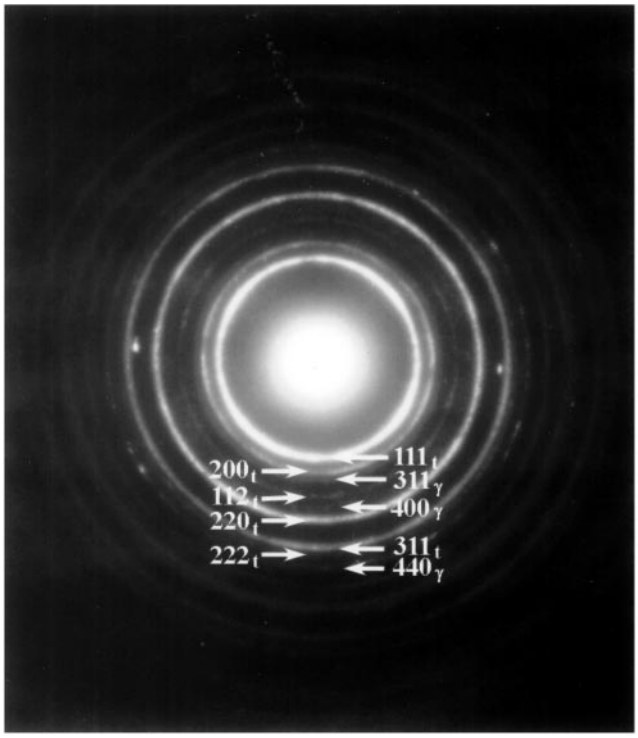

FIG. 6. The selected area diffraction pattern of the specimen sintered at 700 °C confirmed the presence of t-ZrO_2 and $\gamma-Al_2O_3$.

$d = 2.38$, 2.08, and 1.395 Å. While the first two are consistent with $\alpha-Al_2O_3$, other strong peaks of this phase are absent. On the other hand, 2.08 Å corresponds to {112} tetragonal-ZrO_2 while the other two rings match the {311} and {440} of $\gamma-Al_2O_3$ (spinel). Thus, the data are consistent with the presence of a tetragonal-ZrO_2 and $\gamma-Al_2O_3$. While others have reported the formation of a solid solution of alumina in t-ZrO_2 prior to partitioning, there is no clear evidence to support such a conclusion in the present case. No residual $\gamma-Al_2O_3$ could be detected at 800 and 900 °C owing to the presence of strong reflections from the α, t, and m phases. It may be noted that the presence of $\gamma-Al_2O_3$ at 700 °C is consistent with both the TEM as well as the NMR results, while NMR alone reveals a small amount of γ at 800 °C. Average crystallite sizes estimated by XRD are comparable to those seen by TEM.

All samples indicate variations in porosity and hardness between the center and the sides. The density values reported in Table I are the average values of the entire specimen whereas the hardness values are averages of 4–5 readings in the center of the sintered specimen. The density values increase with temperature, as shown in Table I. A significant increase in the theoretical density is expected when the metastable gamma transforms to alpha. Indeed, the sample sintered at 700 °C shows the lowest density and also the least porosity. The hardness values also increase with sintering temperature except for a decrease at 800 °C. This variation reflects the combined contributions of phase transformations and residual porosity. The stable phase, α-alumina is considerably harder (18–20 GPa) than zirconia (8–9 GPa) or $\gamma-Al_2O_3$ (7–9 GPa).

IV. DISCUSSION

A. Phase transformation

The starting powder was x-ray amorphous. The powder used in the present study was heated to 800 °C for 5 min. Balmer *et al.*[3] have shown that crystallization for this composition starts at 850 °C and that phase partitioning starts at 970 °C to yield t-ZrO_2 and $\gamma-Al_2O_3$ followed by m-ZrO_2 and $\alpha-Al_2O_3$ beyond 1100 °C.

TABLE I. A summary of the sintering results.

Specimen	Temperature (°C)	Density (g cm^{-3})	Hardness (GPa)	Phases and grain size (nm) (from XRD)
ZA1	700	4.13	9.5	t-ZrO_2 = 12
ZA2	800	4.60	5.4	t-ZrO_2 = 16, m-ZrO_2 = 26, $\alpha-Al_2O_3$ = 35
ZA3	900	4.76	11.3	t-ZrO_2 = 30, m-ZrO_2 = 30, $\alpha-Al_2O_3$ = 34
ZA4	1000	4.66	12.0	t-ZrO_2 = 24, m-ZrO_2 = 44, $\alpha-Al_2O_3$ = 35
ZA5	1100	4.94	12.7	t-ZrO_2 = 28, m-ZrO_2 = 28, $\alpha-Al_2O_3$ = 55

In contrast, the pressure-sintered sample crystallizes to t-ZrO_2 phase and $\gamma-Al_2O_3$ at 700 °C. The specimen sintered at 800 °C contained $\alpha-Al_2O_3$, indicating that $\gamma \rightarrow \alpha-Al_2O_3$ transformation temperature under 1 GPa pressure is in the range of 700–800 °C. This is in agreement with the results on sintering of $\gamma-Al_2O_3$ at 1 GPa pressure.[6] The 800 °C specimen also shows formation of m-ZrO_2. Again, this temperature is significantly lower than the 1100–1200 °C reported for similar powder.[1,3]

Nucleation enhancement due to pressure

The enhanced transformation is explained below. It is assumed that polymorphic transformation of $\gamma \rightarrow \alpha$ can take place only in pure Al_2O_3. The driving forces in nucleation are chemical free energy ΔG_n/mol at 1 atm pressure, interfacial energy ΔG_i, strain energy due to molar volume mismatch ΔG_s, and free energy due to PV work, ΔG_{pv}.

ΔG_n may be obtained from thermophysical tables while ΔG_{pv} is approximated to $P\Delta\Omega$, where $\Delta\Omega$ = difference in molar volume between γ and α at 1 GPa and room temperature. The approximations in the latter expression lie in ignoring the temperature dependence of the bulk moduli.

ΔG_s, whose importance in retarding transformation has been pointed out earlier,[11] may be estimated by using the expression for a misfitting precipitate with the elastic properties of α-alumina in a matrix of γ-alumina. The moduli of the actual matrix are, of course, unknown, but t-ZrO_2 and $\gamma-Al_2O_3$ have similar moduli. Once again, the room temperature moduli are used, and if one ignores any interaction energy between the hydrostatic pressure and the misfit strain one can write[12]

$$\Delta G_s = 2\mu^{\gamma}\left[\frac{3K^{\alpha}}{3K^{\alpha}+4\mu^{\gamma}}\right]\left[\frac{(\Omega^{\alpha}-\Omega^{\gamma})^2}{3\Omega^{\alpha}}\right], \quad (1)$$

where K is the bulk modulus, μ is the shear modulus, and Ω is the molar volume. The values of the constants used are given in Table II while the energies ΔG_n, ΔG_s, and ΔG_{pv} are listed in Table III. Both ΔG_s and ΔG_{pv} are calculated by using the molar volumes at 1 GPa, assuming a room temperature bulk modulus. The difference in compressibility between γ and α results in a small reduction in the magnitude of these two terms at 1 GPa compared to 1 atm. Since ΔG_s varies as $(\Delta\Omega)^2$ while ΔG_{pv} varies as $\Delta\Omega$, this correction leads to a small overall reduction in the activation barrier.

TABLE II. Values of the constants used for transformation calculations.

	γ	α
E (GPa)[a]	200	390
υ[b]	0.25	0.25
$K\left[=\frac{E}{3(1-2\upsilon)}\right]$	133	253
$\mu\left[=\frac{E}{2(1+\upsilon)}\right]$	80	152
Ω ($\times 10^6$ m^3/mol at 1 atm)	27.94	25.69
Ω ($\times 10^6$ m^3/mol at 1 GPa)	27.73	25.59

[a]*Ceramic Source* (American Ceramics Society, Westerville, OH, 1990), Vol. 6, p. 344.
[b]Assumed for γ. The molar volumes come from the lattice parameters.

The nucleation rate enhancement, R, due to pressure is given by

$$R = \frac{[e^{-\Delta G^*/kT}]_{P=1\text{ GPa}}}{[e^{-\Delta G^*/kT}]_{P=1\text{ atm}}}, \quad (2)$$

where $\Delta G^* = (16\pi)/3\,\Delta G_i^3/(\Delta G_t)^2$ and $\Delta G_i = \gamma/\alpha$ interfacial energy and $\Delta G_t = (\Delta G_n + \Delta G_s + \Delta G_{pv})/\Omega_{\text{average}}$. The activation term due to diffusional attachment to the critical nucleus is assumed to be independent of pressure.

Table III, which lists R at 900–1200 K, shows that the increase in nucleation rate due to pressure is substantial even for what would be considered as low values of interfacial energy. The increase in R with temperature comes about because ΔG_n, the chemical free energy change, decreases and strain energy exerts a greater influence on the overall balance. However, the extrapolation to high temperature becomes increasingly suspect because diffusional relaxation can take place to reduce the misfit between γ and α (and thereby ΔG_s as well).

Thus, we conclude that under hydrostatic pressure, both crystallization as well as transformation of gamma to alpha are accelerated owing to the concurrent change in density.

TABLE III. Values of various energy terms[a] and nucleation rate enhancement at various temperatures.

T (K)	900	1000	1100	1200
ΔG_n, kJ/mol	−15.78	−15.07	−14.30	−13.47
ΔG_s (1 atm), kJ/mol		7.39		
ΔG_s (1 GPa), kJ/mol		6.68		
ΔG_{pv} (1 GPa), kJ/mol		−2.14		
ΔG_t (1 atm), $\times 10^{-8}$ J/mol m^{-3}	−3.13	−2.86	−2.58	−2.27
ΔG_t (1 GPa), $\times 10^{-8}$ J/mol m^{-3}	−4.22	−3.95	−3.66	−3.35
R ($\Delta G_i = 0.1$ J m^{-2})	490	1200	4200	41,000
R ($\Delta G_i = 0.15$ J m^{-2})	10^9	10^{10}	10^{12}	10^{15}

$$\Delta G_t = \frac{\Delta G_n + \Delta G_s + \Delta G_{pv}}{\Omega}$$

[a]JANAF Thermochemical Tables, J. Phys. Chem. Ref. Data **14**, Supplement 1, 156 (1985).

B. Densification

The two important features of the densification behavior that are encountered here are (i) the ability to consolidate at low temperatures, coarse powders that contain micron-sized agglomerates, and (ii) the greater sinterability at 700 °C in the presence of gamma alumina than at higher temperatures when increasing amounts of alpha are present. These observations suggest that crystalline metastable phases in spray-pyrolyzed $ZrO_2-Al_2O_3$ powders may display the same greater sinterability that has been reported in amorphous compositions that were densified to greater than 95% at 650 °C under pressure.[13] Part of the reason may be due to the defective nature of γ-alumina which contains stoichiometric cation vacancies in the spinel structure and which may aid diffusive transport, α-alumina, in contrast, is a highly stable phase with large enthalpies of formation for point defects. In addition, if either of the metastable phases, t-ZrO_2 or $\gamma-Al_2O_3$, contain solute, as suggested by others after rapid solidification[14] and spray pyrolysis,[3] there could be additional concentrations of point defects that aid sintering. The monoclinic zirconia and alpha alumina phases are well known to exhibit little solubility for alumina and zirconia, respectively. Beyond 900 °C the progressive increase in density appears to be related largely to the elimination of voids since the phase contents change only marginally. If one crudely approximates the microstructure to consist of 40 mol% $\alpha-Al_2O_3$ and 60 mol% ZrO_2 equally divided between the tetragonal and monoclinic phases, the theoretical density would be 5.06 g cm^{-3}, giving rise to a relative density of ~98% at 1100 °C.

C. Microstructure

The present results show that superimposed pressure not only reduces the transformation temperatures but also results in a greatly refined and equiaxed microstructure as compared to the free sintered samples.[4] In the latter case, it was shown that the transformation from γ to $\alpha-Al_2O_3$ was accompanied by the formation of single crystal colonies of platelike $\alpha-Al_2O_3$ of several microns with interpenetrating t-ZrO_2 grains of ~0.1–0.2 μm. Such a microstructure was attributed to the growth at high temperatures (1200–1400 °C) of relatively few nuclei of $\alpha-Al_2O_3$. Similar large grained structures evolve when pure $\gamma-Al_2O_3$ transforms to a vermicular $\alpha-Al_2O_3$ in powders prepared by chemical precipitation/decomposition routes.[15] In contrast, the high pressure and low temperatures used in the present study lead to a high nucleation rate and low growth rate of $\alpha-Al_2O_3$ grains, thereby enabling the retention of a nanoscale microstructure. Such equiaxed microstructures have also been reported in $Al_2O_3-Fe_2O_3$ solid solutions[11] in which Fe^{3+} is found to increase the nucleation rate of α from γ.

A further important attribute of the present microstructures is their stability to coarsening. Grain growth in multiphase materials is influenced by the volume fractions of each phase, mutual solubility, and interdiffusivity. Given the presence of three phases, each of which has limited solubility of the minor component, and the low homologous temperatures of processing, it is expected that grain growth would be retarded as observed. While similar stability has been observed[4] between 1200 and 1400 °C for the ZrO_2 phase in loose powders of ZrO_2–40 mol% Al_2O_3, the material of the present study is unique in that the stable grain size of ~50 nm is 4–5 times smaller and applies to $\alpha-Al_2O_3$ as well as to t- and m-ZrO_2. Such stable nanoscale microstructures are desirable if superplastic forming is to be carried out at lower temperatures than currently practiced. It is also encouraging to note that all the samples show the presence of t-ZrO_2, which might be expected to contribute toward transformation toughening.

V. CONCLUSIONS

(1) Application of high pressure leads to lower crystallization, phase partitioning, and phase transformation temperatures for spray-pyrolyzed $ZrO_2-Al_2O_3$ powder owing to large changes in density at each step.

(2) High density nanocrystalline $ZrO_2-Al_2O_3$ composites can be obtained by high pressure sintering of coarse (μm sized) powders.

ACKNOWLEDGMENTS

This work was supported by the U.S. National Science Foundation Grant No. DMR-93 14825 (AKM), the Department of Science and Technology, Government of India (VJ), and U.S. Department of Energy, Basic Sciences Grant No. DE-FG0392ER14240 (CEL). The authors would like to thank Dr. Brian Phillips and the W. M. Keck Foundation for the NMR experiments and Christopher Pike for the sintering experiments.

REFERENCES

1. H. Yoshimatsu, T. Yabuki, and H. Kawasaki, J. Non-Cryst. Solids **100**, 413 (1988).
2. O. Yamaguchi, M. Shirai, and M. Yoshinaka, J. Am. Ceram. Soc. **71**, C-510 (1988).
3. M. L. Balmer, F. F. Lange, and C. G. Levi, J. Am. Ceram. Soc. **77**, 2069 (1994).
4. M. L. Balmer, F. F. Lange, V. Jayaram, and C. G. Levi, J. Am. Ceram. Soc. **78**, 1489 (1995).
5. M. L. Balmer, H. Eckert, N. Das, and F. F. Lange, J. Am. Ceram. Soc. **79**, 321 (1996).
6. R. S. Mishra, C. E. Lesher, and A. K. Mukherjee, J. Am. Ceram. Soc. **79**, 2989 (1996).
7. G. L. Messing, S-C. Chang, and G. V. Jayanthi, J. Am. Ceram. Soc. **76**, 2707 (1993).
8. V. Jayaram, R. S. Mishra, B. Majumdar, C. E. Lesher, and A. K. Mukherjee, in *Proceedings of Particle Science and Technology in the 21st Century* (Engineering Foundation, New York, 1998).
9. F. R. Boyd and J. L. England, J. Geophys. Res. **65**, 741 (1960).
10. R. Dupree, M. H. Lewis, and M. E. Smith, J. Appl. Crystallogr. **21**, 109 (1988).
11. A. D. Polli, F. F. Lange, C. G. Levi, and J. Mayer, J. Am. Ceram. Soc. **79**, 1745 (1996).
12. J. W. Christian, *The Theory of Transformation in Metals and Alloys*, 2nd ed. (Pergamon Press, Oxford, 1975), p. 460.
13. A. S. Gandhi, V. Jayaram, and A. H. Chokshi, Mater. Sci. Forum **243–245**, 227 (1997).
14. V. Jayaram, C. G. Levi, T. Whitney, and R. Mehrabian, Mater. Sci. Eng. **A214**, 65 (1990).
15. F. Dynys and J. W. Halloran, J. Am. Ceram. Soc. **65**, 442 (1982).